RSC Advances

PAPER

View Article Online
View Journal | View Issue

Cite this: *RSC Adv.*, 2020, **10**, 12982

Volatile organic compound gas sensors based on methylammonium lead iodide perovskite operating at room temperature†

Anafi Nur'aini [a] and Ilwhan Oh *[ab]

Received 19th December 2019
Accepted 18th March 2020

DOI: 10.1039/c9ra10703g

rsc.li/rsc-advances

Methylammonium lead iodide ($MAPbI_3$) perovskite thin film has been successfully applied to a volatile organic compound (VOC) gas sensor that can operate at room temperature. In this study, ~100 nm-thick $MAPbI_3$ film shows good reversibility and repeatability as a VOC gas sensor. The resistance of the $MAPbI_3$ film substantially decreases when it is exposed to VOC vapour and recovers back to high resistance when the VOC gas is removed. Adsorption of VOC gas molecules to vacancies in $MAPbI_3$ film might lead to charge trap passivation. The VOC sensor based on perovskite thin film is tested in terms of film thickness, applied bias voltage, and polarity of VOC. We expect that our VOC gas sensor based on solution-processed $MAPbI_3$ operating at room temperature has potential to be developed as a low cost and low power smart gas sensor.

Introduction

Gas sensing technology has a crucial role in air condition monitoring,[1] safety instruments in laboratories and industry,[2] and exhalation analysis for disease diagnosis.[3,4] Some key requirements for gas sensors are sensitivity, fast response, room temperature operation, and low-cost fabrication. Regarding the principle of detection, various gas sensor types can be categorized into electrochemical types,[5] catalytic types,[6] metal oxide types,[7–10] and infrared types.[10] Recently, due to the emergence of smart sensor technology, the requirement is emphasized on low power and small size devices.[11,12] Unfortunately, those requirements are difficult to meet in a specific sensor type. For example, to keep the high operating temperature, metal oxide gas sensor consumes high power although its sensing element can be fabricated in a microscale device.[10]

Volatile organic compound (VOC) gases contribute to air pollution in environment,[13] which is more severe in indoor space. Nevertheless, some VOC gases are proven to be disease biomarkers.[3,14] In abnormal metabolism, VOC can be produced and disposed through exhales breath.[3] Unlike healthy people, lung cancer patients have different VOC profile in exhale breath.[14] Moreover, VOCs are omnipresent in our daily lives due to their high volatility and have been commonly used for household products such as paints, aerosol sprays, moth repellents, pesticides, adhesive, and air fresheners. However, VOCs can stimulate health problems such as respiratory diseases,[15] eye irritation,[16] skin allergy,[17] fatigue,[18] and central nervous system disorder.[19]

Several metal oxide semiconductors have been widely utilized as sensing materials in chemical gas sensors, including SnO_2,[20] Co_3O_4,[21] ZnO,[22] and TiO_2.[23] Traditional metal oxide materials need high temperature (~250–300 °C) to operate,[9] although recently some metal oxide materials are developed to be operated in lower temperature.[24] Finding a new semiconductor material for gas sensor that can operate at room temperature is a relevant topic.

Metal halide perovskites are popular as solar cell devices. The efficiency of solar cell based on metal halide perovskite increases from 3.8% in 2009 to 23.3% in 2018.[25] Molecular formula of perovskite is AMX_3. A is organic cation ($CH_3NH_3^+$, $CH_3\ CH_2NH_3^+$, $HC(NH_2)_2^+$), M is metal cation (Ge^{2+}, Sn^{2+}, Pb^{2+}), and X is halogen anion (F^-, Cl^-, Br^-, I^-).[26] Six halogen atoms (X) form octahedral structure with metal M atom located in the centre, while cation A is located at the centre of eight octahedral structure.[26] Unlike most of metal oxide semiconductors, organic metal halide perovskites exhibit a relatively high conductivity even at room temperature.[27] Moreover, perovskite layer can be fabricated by simple and low-cost solution deposition process.[28]

Recently, metal halide perovskites have emerged as material for lasers, light-emitting diodes, field-effect transistors, and gas sensors.[26,27] In 2013, Zhao's group showed that the colour of $MAPbI_3$ film was bleached when it passed through an open bottle containing 3% NH_3 solution.[29] The colour change was reversible when $MAPbI_3$ film was taken away from the bottle.[29] In other reports, through a chemiresistive technique, $MAPbI_3$ perovskite was utilized as gas sensors toward various chemical

[a]Department of IT Convergence Engineering, Kumoh National Institute of Technology, Gumi, Gyeongbuk, South Korea 39177. E-mail: ioh@kumoh.ac.kr

[b]Department of Applied Chemistry, Kumoh National Institute of Technology, Gumi, Gyeongbuk, South Korea 39177

† Electronic supplementary information (ESI) available. See DOI: 10.1039/c9ra10703g

vapours, such as ammonia,[30] oxygen,[31] and NO_2.[32] When $MAPbI_3$ film was exposed to target gas molecules, its molecules might fill vacancies in $MAPbI_3$ film then substantially elevate conductivity of $MAPbI_3$.[30–32] In contrast when an inert gas reaches $MAPbI_3$ film, its molecules will knock out target gas molecules and recreate vacancies, thus conductivity of $MAPbI_3$ decreases.[30–32] Those reports indicate that $MAPbI_3$ can detect not only reducing gas but also oxidizing gas.

Modified halide perovskite such as $CH_3NH_3PbI_{3x}(SCN)_x$ was successfully employed as NO_2 and acetone gas sensor with high sensitivity.[33] Kakavelakis group reported that $CH_3NH_3PbI_{3-x}Cl_x$ could operate as ozone gas sensor at room temperature.[34] On the other hand, Chen and co-workers applied all-inorganic $CsPbBr_3$ materials to detect ethanol, acetone, and oxygen with good sensitivity and stability.[35] Nonetheless, organic metal halide perovskite especially $MAPbI_3$ has not been extensively studied for VOCs detection.

In this paper, we fabricate a gas sensor based on a thin film $MAPbI_3$ and show that perovskite-based device is a decent gas sensor toward various VOCs. Through conductivity and photoluminescence measurements, we propose a sensing principle that charge trap passivation model fits better than depletion layer model in traditional metal oxide sensors. Furthermore, we adjust and optimize various experimental parameters such as film applied bias, thickness, and polarity of gas molecules.

Results and discussion

Perovskite-based sensing device was fabricated *via* conventional microfabrication process (refer to Experimental details section). In brief, a gold interdigitated electrode (IDE) pattern was fabricated using photolithography and wet-etch on a glass substrate (Fig. 1a). Finger width was 100 μm and space width was 50 μm. Perovskite solution was deposited by a spin-coating process. After deposition, perovskite film looked uniform and mirror-like (Fig. 1b).

Current–time response of perovskite film gas sensor was measured by applying voltage bias to the interdigitated electrode. Measurement process was conducted at room temperature in a small chamber as shown in Fig. 1c. A known concentration of target gas was injected into the chamber. After measuring sensor response, inert gas was injected to recover perovskite film sensor. Measured current response was transformed into normalized response (R) by following equation:[31]

$$R = \frac{\Delta I}{I_0} = \frac{I - I_0}{I_0}$$

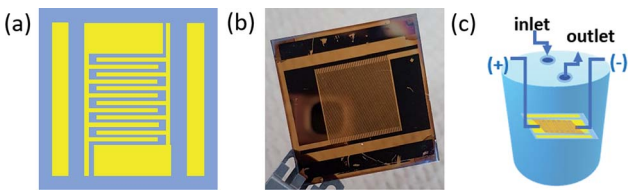

Fig. 1 (a) Interdigitated electrode (IDE) (b) perovskite film on the IDE, (c) gas sensing measurement setup.

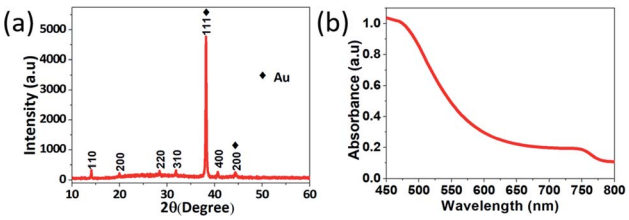

Fig. 2 (a) X-ray diffraction (XRD) spectra and (b) UV-visible spectroscopy of $MAPbI_3$ film.

where I is current during target gas exposure and I_0 is background current without target gas.

Perovskite material was characterized by X-ray diffraction and UV-visible spectroscopy. X-ray diffraction results in Fig. 2a confirms the formation of $MAPbI_3$ tetragonal phase.[36] Peaks at 14.08°, 19.98°, 28.4°, 31.92°, and 40.68° correspond to (110), (200), (220), (310), and (400) crystal planes respectively. By Scherrer equation, the average grain was calculated to be 44 nm. As Au interdigitated electrode was employed as a substrate, additional peaks at 38.2° and 44.38° correspond to (111) and (200) Au crystal planes. For UV-visible spectrum in Fig. 2b, absorption onset around 750–800 nm is consistent with the bandgap of $MAPbI_3$. Bandgap energy is determined to be 1.58 eV from $(\alpha h\nu)^2$ *vs.* $h\nu$ graph (Fig. S1†). This value is consistent with reported bandgap of $MAPbI_3$.[37]

Top-view and cross-section images from SEM are shown in Fig. 3a and b. Fig. 3a shows small grains size and grain boundaries of perovskite film. Perovskite film thickness is ~100 nm (Fig. 3b) and surface roughness is 15 nm (Fig. S2†). Small grains size is preferred as gas sensing application because of high surface-to-volume ratio, high sensitivity, and fast response. Grain boundaries help target gas to penetrate to perovskite film.

Fig. 4a shows a dynamic response–time graph of perovskite gas sensor towards 10 000 ppm ethanol vapour. Significant responses emerge when perovskite film is exposed to ethanol vapour and recover to the initial background when ethanol vapour is replaced with inert gas. As shown in Fig. 4a, perovskite film has response time (t_{rs}) of 66 seconds and recovery time (t_{rc}) of 67 seconds, which are faster than other type gas sensors.[38] Perovskite film shows successive responses during four cycles toward ethanol. Thus, ethanol exposure seems not to damage the structural integrity of perovskite film. Interaction between perovskite film and ethanol is assumed to be mainly

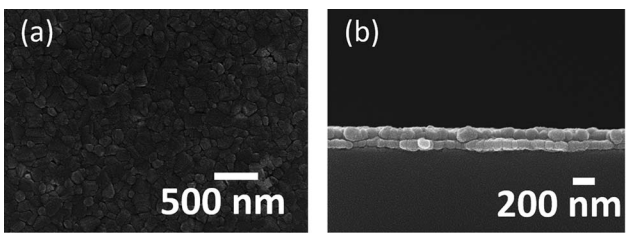

Fig. 3 Scanning electron microscope (SEM) images for (a) top-view, and (b) cross-section of $MAPbI_3$ film.

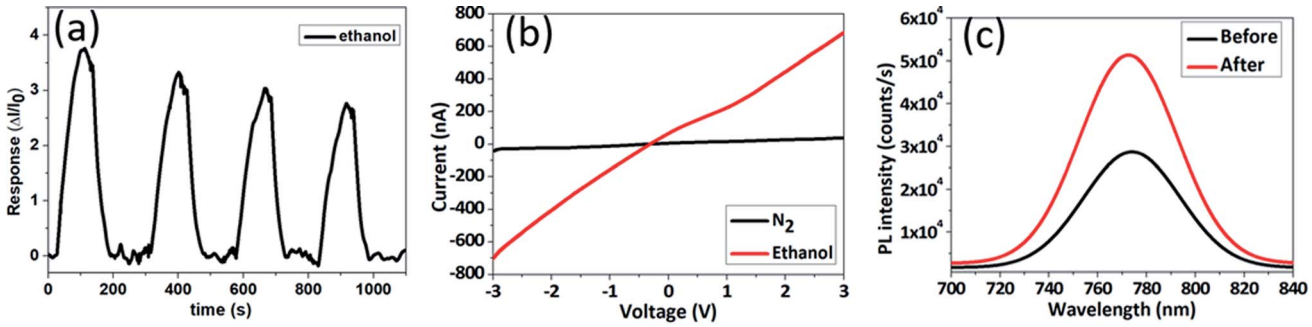

Fig. 4 (a) Response–time graph of $MAPbI_3$ film when ethanol gas was turned ON and OFF, (b) *I–V* curve of $MAPbI_3$ during exposure towards nitrogen and ethanol gas, (c) photoluminescence intensity of perovskite film before and after ethanol gas exposure.

physisorption and limited on perovskite grain boundaries. However, as measurement repeat, peak heights become lower. This damping probably comes from a slow side reaction between the perovskite crystal and the target gas molecules. We will discuss sensing mechanism in more detail later.

We further investigate into sensing mechanism of the perovskite gas sensor. As a comparison, the sensing mechanism of conventional metal oxide semiconductor is worth to be considered. Metal oxide semiconductor absorbs oxygen molecules from ambient air.[39] Oxygen molecules attract electrons from metal oxide to form O_2^-, O^-, or O^{2-} ions, then form a depletion layer that reduces the conductivity of metal oxide semiconductor.[8,9,39] In contrast, our experiment reveals that exposure of perovskite sensor to ambient oxygen increases the conductivity of $MAPbI_3$ film. Fig. S3† shows *I–V* curve of $MAPbI_3$ film responses toward nitrogen and ambient air under voltage bias −3 V to 3 V. Regarding Fig. S3,† the conductivity of $MAPbI_3$ film is much higher during ambient air exposure than during nitrogen exposure. Similarly, Fig. 4b presents *I–V* curve of $MAPbI_3$ film that is exposed to nitrogen and ethanol gas under voltage bias −3 V to 3 V. Fig. 4b proves that ethanol exposure substantially promotes the conductivity of perovskite film. This observation proves that the sensing mechanism of $MAPbI_3$ film is different from conventional metal oxide sensors.

An alternative sensing mechanism involves passivation of charge trap state.[31] $MAPbI_3$ is well known to contain iodine vacancies (V_I). There are two types of iodine vacancies, $V_{I(a)}$ and $V_{I(b)}$. $V_{I(a)}$ are located in MA-I layers and $V_{I(b)}$ are located in Pb–I layers.[40] As MA-I layer is a termination layer of $MAPbI_3$, most of iodine vacancies are located on the surface, interfacial site, and grain boundaries. Due to organic solvent evaporation during annealing process in film formation, a high density of crystal defects can be formed.[41] These defects act as trap states. In pristine film, electrons can fall from conduction band into the trap states. As a consequence, perovskite film has low conductivity. Crystal defects on the surface work as active sites. Absorbing target gas molecules can passivate iodine vacancies and release free trapped charges. Therefore, electrons that are trapped in iodine vacancies can be restored into the conduction band. At that moment, the conductivity of perovskite film increases. In contrast, the absorbed inert gas molecules expel the target gas molecules and re-establish crystal defects of perovskite film. This sensing mechanism is supported by the photoluminescence (PL) measurement. Fig. 4c presents PL measurements of perovskite film before and after ethanol gas exposure. Before ethanol exposure, high density of crystal defect is indicated by low PL intensity. After ethanol exposure, crystal defect density becomes lower and crystallinity of perovskite improves, thus PL intensity increases. This result indicates that electronic quality of perovskite film is improved, supporting the trap state passivation hypothesis.[34,42]

To understand the effect of applied bias on sensor performance, perovskite film was tested under different applied bias. Biasing technique has been applied to improve zinc oxide (ZnO)

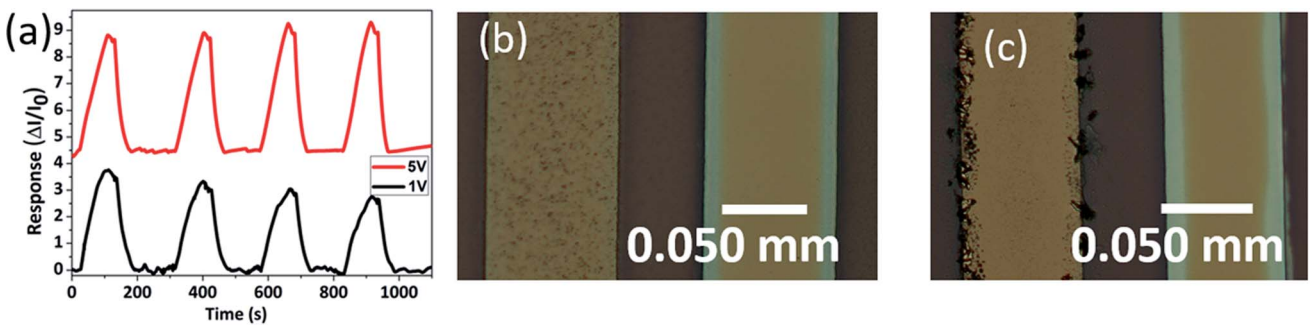

Fig. 5 (a) Sensor response under different applied bias voltage (1 V and 5 V). Optical image of $MAPbI_3$ (magnification 1000×) after suppressing under (b) 1 V voltage bias (c) 5 V voltage bias for 10 minutes. All perovskite films were exposed by 10 000 ppm of ethanol gas.

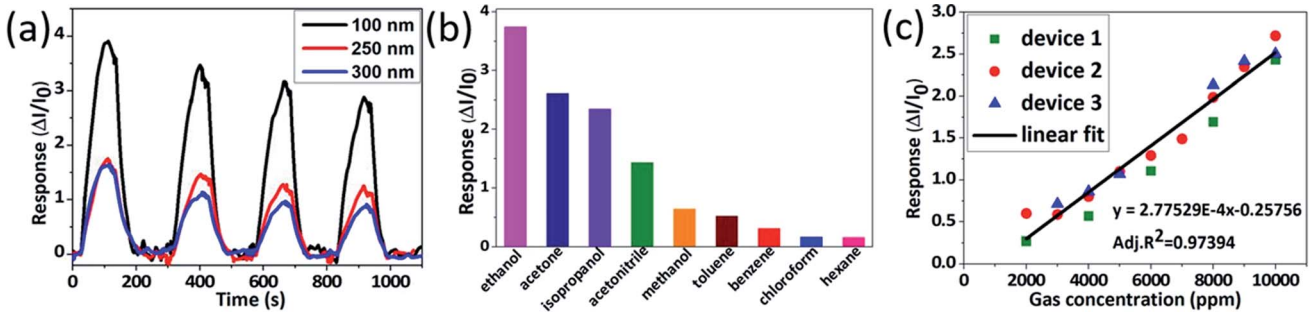

Fig. 6 (a) Sensor response with different thickness (100 nm, 250 nm, and 300 nm), (b) comparison of $MAPbI_3$ responses towards 10 000 ppm of each gas, (c) sensor response of multiple perovskite sensor devices *versus* gas concentration.

performance as hydrogen sensor,[43] thus this technique might be worked as well for perovskite sensor. Fig. 5a shows response–time graph of $MAPbI_3$ film under 1 V and 5 V. Different applied bias produces a similar trend of response–time graph, but the absolute current of $MAPbI_3$ film under 5 V is one order magnitude higher than under 1 V (Fig. S4†). A higher level of absolute current at 5 V leads to smaller baseline noise level compare to at 1 V. However, at 5 V perovskite film is damaged from ion migration and/or faradaic reactions. As a comparison, Fig. 5c and d show optical image of $MAPbI_3$ film after applying different bias for 10 minutes under similar gas exposure (10 000 ppm ethanol). $MAPbI_3$ film looks intact under 1 V bias. In contrast, 5 V bias exhibits severe damage to $MAPbI_3$ film especially near cathode, which might be caused by iodide migration and PbI_2 formation.[44] From these experiments, we understand that sensing response can be improved, but we should keep low voltage bias to prevent perovskite film degradation.

We further tried to figure out and optimized perovskite gas sensor. To investigate the effect of perovskite film thickness on sensor response, we fabricated perovskite films from different perovskite precursor concentrations. Perovskite film cross-section and top-view are depicted in Fig. S5 and S6.† Those figures demonstrate that higher concentration produces thicker film and bigger grains size. 0.5 M, 1.0 M, and 1.5 M precursor solution produces perovskite film thickness ~100 nm, 0–250 nm, and ~300 nm respectively. Fig. 6a displays a response–time graph of $MAPbI_3$ film with different thickness toward similar gas concentration (10 000 ppm) exposure at room temperature. Thinner perovskite film produces a higher response. Film thickness has a dependence towards sensitivity of sensing film. The sensitivity drops as the thickness increase.[45] Two factors possibly play roles here. First, target gas molecules might penetrate only in the upper part of thicker perovskite film, which produces a lower response. Second, bigger grains in thicker perovskite film lead to lower density of grain boundaries. Therefore, the amount of the target gas molecules that can penetrate the film will be reduced, resulting in a lower response. We have tried to further decrease the film thickness by lowering perovskite concentration. For 0.25 M $MAPbI_3$, the film was not uniform which lead to film damage (Fig. S7a†). As a consequence, this film had a poor response (Fig. S7b†).

As VOC sensor, perovskite gas sensor devices were tested toward a range of typical organic VOCs. We compared $MAPbI_3$ film response to VOC polar gases (ethanol, acetone, isopropanol, acetonitrile, and methanol) and VOC non-polar gases (toluene, benzene, chloroform, and hexane). Among them, ethanol presents the highest response, whereas hexane presents the lowest. Generally, the perovskite sensor is more sensitive to polar gas than non-polar gas. We can assume that polar gas molecules stick stronger to $MAPbI_3$ defect sites, as $MAPbI_3$ perovskite itself is a polar ionic crystal, resulting in higher responses (Fig. 6b).

Multiple devices were fabricated and measured in a range of gas concentrations as shown in Fig. 6c. This result confirms high reproducibility of our gas sensing device. The calibration graph shows good linearity between sensor response and gas concentration. According to Fig. 6b, the sensitivity of perovskite sensor is 3×10^{-4} ppm^{-1}. Limit of detection (LOD) can be calculated by following equation:[46]

$$\mathrm{LOD} = 3\frac{S_y}{b}$$

S_y is the standard deviation of y-residuals and b is the sensitivity from the calibration graph.[46] Quantitatively, the LOD of our perovskite film is ~1300 ppm which still lower than 3300 ppm of IDLH (immediately dangerous to life or health) ethanol concentration.[21] This sensitivity value is low for some application (*e.g.*, exhalation analysis for disease diagnosis), but some possible improvement such as gas preconcentration or electric amplification can be made to maximize the sensitivity.

Finally, we have applied the perovskite gas sensor to detect VOC from commercial chemical products such as nail polish remover and soju (famous Korean liquor). Nail polish remover contains 30–60% acetone,[47] while soju contains 20–25% ethanol.[48] Fig. S8 and S9† show the electrical response of perovskite as it exposed to nail polish remover and soju vapour. Perovskite gas sensor exhibits good response to both commercial products. Those experiments proved that $MAPbI_3$ perovskite gas sensor has a great potential to be utilized as ambient VOC detector in daily life.

Conclusions

In summary, a solution-processed $MAPbI_3$ film was utilized as sensing material in VOCs gas sensor that can respond and recover fast at room temperature. The responses of the perovskite gas sensor originated from the conductivity change in the presence and absence of target gas. A sensing mechanism of the perovskite sensor has been proposed which is different from that of conventional metal oxide gas sensors. Charge trap passivation process by target gas adsorption seems to alter the $MAPbI_3$ film conductivity. Thinner layer and lower applied bias are preferred due to higher electrical response and slow degradation of $MAPbI_3$ film. In addition, selectivity test reveals that the $MAPbI_3$ film is more sensitive to polar VOC gases than to non-polar VOC gases. This work offers an opportunity for $MAPbI_3$ perovskite to be developed as low-cost and low-power gas sensor that can operate at room temperature.

Experimental details

Fabrication of interdigitated electrode (IDE)

1 mm thick bare glass (2.5 × 2.5 cm) was cleaned by immersing into piranha solution (3 : 1 v/v of H_2SO_4 and H_2O_2) for 3 hours at 60 °C and was subsequently treated by oxygen plasma for one minute. Cr (15 nm) and Au (80 nm) were deposited on top of bare glass using a thermal evaporator. Photolithography and wet etch processes were used to form interdigitated electrode pattern. Photoresist AZ GXR 601 was spin-coated above metal film, then followed with soft bake for 90 seconds at 90 °C. After that, the sample was covered by IDE pattern mask and exposed by UV lamp for 16 seconds. The sample was annealed for 90 seconds at 90 °C. Developer AZ MIF 300 was employed to develop for 30 seconds. Next, oxygen plasma treatment was applied for 2 minutes to remove residues. Wet etching processes of Au and Cr were done using Au etchant for 20 seconds and Cr etchant for 15 seconds. Photoresist layer was removed by acetone.

Perovskite film formation

Perovskite solution was made by CH_3NH_3I and PbI_2 powder (1 : 1) mol ratio to DMSO in γ-butyrolactone. The perovskite solution was stirred with 300 rpm at 60 °C for minimum 1 hour, then it was filtered using 0.50 μm nylon filter to obtain a clear solution. For deposition process, it was done in a glove box with N_2 ambient. 300 μL perovskite solution was dropped on the top of an interdigitated electrode (IDE) and was spun using spin coater with 1000 rpm for 40 seconds and 5000 rpm for 20 seconds. During the last 10 seconds, 800 μL toluene was dropped on the top of perovskite surface as anti-solvent. Perovskite film was annealed at 100 °C for 10 minutes.

Characterization and sensor testing

X-ray diffraction (XRD) pattern of $MAPbI_3$ film was recorded by X-MAX Rigaku diffractometer with Cu Kα radiation from 3° to 60°. Scanning electron microscope (SEM) images of $MAPbI_3$ film were taken by MAIA III-TESCAN. Atomic force microscopy (AFM) was performed by Park SYSTEM/XE-100. UV-visible of UV $MAPbI_3$ film was measured by OPTIZEN 3220 UV absorption spectroscopy with wavelength range from 450 nm to 800 nm. Optical image observation was performed by HIROX/KH-8700 digital microscope.

Before gas sensing test, one litre of 10 000 ppm target gas was prepared in a Tedlar bag. Volatile organic compound (liquid) was injected into a Tedlar bag. VOC liquid was diluted by filling the bag with one litre of N_2 gas. The amount of VOC (liquid) was calculated correctly correspond to molecular weight of VOC, its density, final volume of dilution, and final concentration.

Gas sensing test was conducted by isolating $MAPbI_3$ film in a cylinder chamber ($V_{cylinder}$ = 16 ml). Interdigitated electrode was connected to potentiostat electrodes. Potentiostat PalmSens 4 was employed to record electrical response of $MAPbI_3$ film. During gas sensing test, target gas was injected into the chamber for 90 seconds (rate gas 20 ml min^{-1}), then N_2 was injected right after target gas was stopped.

Conflicts of interest

There are no conflicts to declare.

Acknowledgements

I. O. acknowledges the support from the National Research Foundation (NRF) of Korea (NRF-2016R1A2B4011046).

References

1 A. L. Clements, W. G. Griswold, A. Rs, J. E. Johnston, M. M. Herting, J. Thorson, A. Collier-Oxandale and M. Hannigan, *Sensors*, 2017, **17**, 2478.
2 M. Willett, *Sensors*, 2014, **14**, 6084–6103.
3 A. H. Jalal, F. Alam, S. Roychoudhury, Y. Umasankar, N. Pala and S. Bhansali, *ACS Sens.*, 2018, **3**, 1246–1263.
4 D. Kohl, *J. Phys. D: Appl. Phys.*, 2001, **34**, R125–R149.
5 M. A. H. Khan, M. V. Rao and Q. Li, *Sensors*, 2019, **19**, 905.
6 J. Liu, T. Han, B. Sun, L. Kong, Z. Jin, X. Huang, J. Liu and F. Meng, *Catalysts*, 2016, **6**, 210.
7 A. S. Zuruzi and N. C. MacDonald, *Adv. Funct. Mater.*, 2005, **15**, 396–402.
8 A. Kolmakov and M. Moskovits, *Annu. Rev. Mater. Res.*, 2004, **34**, 151–180.
9 C. Wang, L. Yin, L. Zhang, D. Xiang and R. Gao, *Sensors*, 2010, **10**, 2088–2106.
10 G. F. Fine, L. M. Cavanagh, A. Afonja and R. Binions, *Sensors*, 2010, **10**, 5469–5502.
11 D. Antolin, N. Medrano, B. Calvo and F. Perez, *Sensors*, 2017, **17**, 365.
12 V. Jelicic, M. Magno, D. Brunelli, G. Paci and L. Benini, *IEEE Sensor. J.*, 2013, **13**, 328–338.
13 H. Huang, Y. Xu, Q. Feng and D. Y. C. Leung, *Catal. Sci. Technol.*, 2015, **5**, 2649–2669.
14 S. Das, S. Pal and M. Mitra, *J. Med. Biol. Eng.*, 2016, **36**, 605–624.

15 J. Shuai, S. Kim, H. Ryu, J. Park, C. K. Lee, G. B. Kim, V. U. Ultra Jr and W. Yang, *BMC Publ. Health*, 2018, **18**, 528.
16 A. Hempel-Jorgensen, S. K. Kjaergaard, L. Molhave and K. H. Hudnell, *Arch. Environ. Health*, 1999, **54**, 416–424.
17 K. Ahn, *J. Allergy Clin. Immunol.*, 2014, **134**, 993–999.
18 D. A. Otto, H. K. Hudnell, D. E. House, L. Molhave and W. Counts, *Arch. Environ. Health*, 1992, **47**, 23–30.
19 S. Genc, Z. Zadeoglulari, S. H. Fuss and K. Genc, *J. Toxicol.*, 2012, **2012**, 782462.
20 T. Kida, K. Suematsu, K. Hara, K. Kanie and A. Muramatsu, *ACS Appl. Mater. Interfaces*, 2016, **8**, 35485–35495.
21 T. Lin, X. Lv, Z. Hu, A. Xu and C. Feng, *Sensors*, 2019, **19**, 233.
22 S. Bhatia, N. Verma and R. K. Bedi, *Results Phys.*, 2017, **7**, 801–806.
23 K. Zakrzewska and M. Radecka, *Nanoscale Res. Lett.*, 2017, **12**, 89.
24 Z. Li, H. Li, Z. Wu, M. Wang, J. Luo, H. Torun, P. Hu, C. Yang, M. Grundmann, X. Liu and Y. Fu, *Mater. Horiz.*, 2019, **6**, 470–506.
25 Z. Zhu, Q. Sun, Z. Zhang, J. Dai, G. Xing, S. Li, X. Huang and W. Huang, *J. Mater. Chem. C*, 2018, **6**, 10121–10137.
26 S. T. Ha, R. Su, J. Xing, Q. Zhang and Q. Xiong, *Chem. Sci.*, 2017, **8**, 2522–2536.
27 B. Gebremichael, G. Alemu and G. Tessema Mola, *Phys. B*, 2017, **514**, 85–88.
28 A. B. Djurišić, F. Z. Liu, H. W. Tam, M. K. Wong, A. Ng, C. Surya, W. Chen and Z. B. He, *Prog. Quantum Electron.*, 2017, **53**, 1–37.
29 Y. Zhao and K. Zhu, *Chem. Commun.*, 2014, **50**, 1605–1607.
30 C. Bao, J. Yang, W. Zhu, X. Zhou, H. Gao, F. Li, G. Fu, T. Yu and Z. Zou, *Chem. Commun.*, 2015, **51**, 15426–15429.
31 M. A. Stoeckel, M. Gobbi, S. Bonacchi, F. Liscio, L. Ferlauto, E. Orgiu and P. Samori, *Adv. Mater.*, 2017, **29**, 1702469.
32 X. Fu, S. Jiao, N. Dong, G. Lian, T. Zhao, S. Lv, Q. Wang and D. Cui, *RSC Adv.*, 2018, **8**, 390–395.
33 Y. Zhuang, W. Yuan, L. Qian, S. Chen and G. Shi, *Phys. Chem. Chem. Phys.*, 2017, **19**, 12876–12881.
34 G. Kakavelakis, E. Gagaoudakis, K. Petridis, V. Petromichelaki, V. Binas, G. Kiriakidis and E. Kymakis, *ACS Sens.*, 2018, **3**, 135–142.
35 H. Chen, M. Zhang, R. Bo, C. Barugkin, J. Zheng, Q. Ma, S. Huang, A. W. Y. Ho-Baillie, K. R. Catchpole and A. Tricoli, *Small*, 2018, **14**, 1702571.
36 A. Arakcheeva, V. Svitlyk, E. Polini, L. Henry, D. Chernyshov, A. Sienkiewicz, G. Giriat, A. Glushkova, M. Kollar, B. Náfrádi, L. Forro and E. Horváth, *Acta Crystallogr., Sect. B: Struct. Sci., Cryst. Eng. Mater.*, 2019, **75**, 361–370.
37 A. M. Leguy, P. Azarhoosh, M. I. Alonso, M. Campoy-Quiles, O. J. Weber, J. Yao, D. Bryant, M. T. Weller, J. Nelson, A. Walsh, M. van Schilfgaarde and P. R. Barnes, *Nanoscale*, 2016, **8**, 6317–6327.
38 D. Acharyya and P. Bhattacharyya, *Sens. Actuators, B*, 2016, **228**, 373–386.
39 K. Arshak, E. Moore, G. M. Lyons, J. Harris and S. Clifford, *Sens. Rev.*, 2004, **24**, 181–198.
40 L.-y. Wei, W. Ma, C. Lian and S. Meng, *J. Phys. Chem. C*, 2017, **121**, 5905–5913.
41 J. Huang, Y. Yuan, Y. Shao and Y. Yan, *Nat. Rev. Mater.*, 2017, **2**, 17042.
42 R. Brenes, D. Guo, A. Osherov, N. K. Noel, C. Eames, E. M. Hutter, S. K. Pathak, F. Niroui, R. H. Friend, M. S. Islam, H. J. Snaith, V. Bulović, T. J. Savenije and S. D. Stranks, *Joule*, 2017, **1**, 155–167.
43 T. F. Choo, N. U. Saidin and K. Y. Kok, *R. Soc. Open Sci.*, 2018, **5**, 172372.
44 Z. Xiao, Y. Yuan, Y. Shao, Q. Wang, Q. Dong, C. Bi, P. Sharma, A. Gruverman and J. Huang, *Nat. Mater.*, 2015, **14**, 193–198.
45 F. Hossein-Babaei and M. Orvatinia, *Sens. Actuators, B*, 2003, **89**, 256–261.
46 A. Shrivastava and V. Gupta, *Chronicles Young Sci.*, 2011, **2**, 21.
47 M. Bernstein, *US Pat.*, 4735798, 1988.
48 W. Chung, *Alcohol Alcohol.*, 2004, **39**, 39–42.